arXiv:1002.0821v1 [cond-mat.mtrl-sci] 3 Feb 2010

Statistics of acoustic emission in paper fracture: precursors and criticality

J. Rosti, J. Koivisto, M.J. Alava

Department of Applied Physics, Helsinki University of Technology, FIN-02015 HUT, Finland

E-mail: jro@fyslab.hut.fi

PACS numbers: 62.20.M-,05.40.-a, 46.50+a

Abstract.

We present statistical analysis of acoustic emission (AE) data from tensile experiments on paper sheets, loading mode I, with samples broken under strain control. The results are based on 100 experiments on unnotched samples and 70 samples with a long initial edge notch. First, AE energy release and AE event rates are considered for both cases, to test for the presence of "critical points" in fracture. For AE energy, no clear signatures are found, whereas the main finding is that the event rate diverges when a sample-dependent "critical time" of the maximum event rate is approached. This takes place after the maximum stress is reached. The results are compared with statistical fracture models of heterogenous materials. We also discuss the dependence of the AE energy and event interval distributions on average event rates.

1. Introduction

Fracture of heterogenous material exhibits scaling properties familiar from statistical physics. Scaling laws of energy release and fluctuations in temporal statistics tempts one to interpret fracture via concepts of criticality and phase transitions. However, simple models have failed to convey the phenomenology and the origins of observed scaling laws are lacking. In this work we have performed extensive set of tensile experiments on paper sheets in order to discuss the concept of criticality in mode I loading with imposed strain. [1, 2].

Typical stress-strain curve in tensile fracture of paper samples exhibits some non-linearity before the maximum stress, σ_c. This is a result of both plastic, irreversible deformation and to a much lesser degree of loss of elastic stiffness, or damage accumulation [3]. We study the damage accumulation by using "acoustic emission" (AE). This is the release of elastic energy due to microcracking on various scales ranging from far below the fiber size to, perhaps, millimeters as in the individual advances made by a notch in a tensile test. AE studies have been done in a wide variety for materials in science and engineering [4]. The common features in most are that the material failure process is complicated and disorder is present in the structure. Numerous studies have elucidated the statistical laws that describe AE. In general, these relate to usual mode I or mode III -type loading conditions, and the common feature is that they exhibit*scalefree* features. The probability distribution function (pdf) of event energies follows most often a power-law, with exponents in the range $\beta = 1 \ldots 2$. The event intervals are, similarly, found to obey such fat-tailed pdf's. [5, 6, 7, 2, 8]

Here we consider paper as a test material or case of critical divergences during the fracture in the presence of structural randomness. This idea of criticality can be formulated in various ways, but essentially it implies the presence of a finite time singularity, so that a quantity such as the AE energy release during the approach of the failure becomes a function of $1/(t_c - t)$ where t_c is the lifetime. In the following, we focus on the non-stationary AE signal from tensile experiments with imposed strain and study energy and event statistics of AE near the failure. We study in detail local averages of e.g released acoustic emission energy when t_c, or critical point, is approached. The relation between critical point t_c and the time at the maximum stress σ_c is discussed.

The total number of observed acoustic emission events in all experiments is 800921. The high number of events in a single experiment (few thousands of events, comparable to rock and concrete fracture experiment cases [9, 10]) combined with the large number of samples allows us to study the non-stationarity of the acoustic emission signal.

What kind of AE signature is produced by driving the fracture, e.g. by imposing a constant strain or creep stress, is not well understood. Thus, understanding the statistical properties of the acoustic emision and fracture precursors could provide a way to distinguish between different modes of loading. One possible application of this is in creating analogies with experimental findings in seismicity [11].

The main result of the analysis is that we can distinguish two fundamental cases:

the dynamics in samples without a dominating notch and dynamics in the presence of a large defect with slow, stable crack growth. In the former case, there is evidence of such a divergence, upon approach of a sample-dependent critical time. This takes place after the sample maximum stress is reached. A qualitative explanation is perhaps offered by the dynamics which stems from the nucleation and growth of a dominating microcrack.

To discuss the divergence, we consider simple models of statistical fracture. We show that variants of a minimal quasi-static fracture (random fuse network, RFN) model do not exhibit such features as the data. It is well-known that the RFN and other models do not reproduce quantitatively e.g. the exponents that characterize AE statistical properties. It also turns out that the divergence is not found in such models, however a RFN variant with gradual failure gets slightly closer [12].

The structure of the rest of this paper is as follows. In Section 2, we discuss the background and details of the experiments. Section 3 presents various aspects of the data analysis, and is finished with a subsection on modeling attempts. Section 4 presents discussion and summary.

2. Experiments

Normal copy paper samples were tested in the cross direction on a mode I laboratory testing machine of type MTS 400/M. The deformation rate $\dot{\epsilon}$ was 10 mm min^{-}1. The AE system consisted of a piezoelectric receiver, a rectifying amplifier and continuous data-acquisition. The data-acquisition was free of deadtime. The stress was measured simultaneously directly from MTS 400/M using same time-resolution as AE-signal; thus the accuracy of time synchronization of the acoustic emission and stress-strain curves was below 10 μs.

During the experiment, we acquired bi-polar acoustic amplitudes simultaneously on two channels by piezocrystal sensors, as a function of time. Two transducers were attached directly to paper without a coupling agent. Each channel has 12-bit resolution and a sampling rate of 312 000 Hz. The transmission time from event origin to sensors is in the order of 5 μs. The acoustic channels were first amplified and after that held using sample-and-hold circuit.

70 samples had initial notches of size 10 mm to achieve stable crack growth and 100 samples were intact. Sample geometry was 150 $\times$ 50 mm^2. Samples were tested in standard conditions: temperature of 22 degree in Celcius and relative humidity of 30%.

The acoustic time-series was post-processed after the measurement by detection of continuous and coherent events, and the calculation of an event energy E_i is done as the integral of squared amplitudes within the event: $E_i = \int A^2(t')dt'$. The event arrival time t_i was taken from an instant when the amplitude raises above the threshold level. Dynamic range of the measurement device was 54 dB. The ensuing discrete set of events is characterized by set of pairs: $\{(t_1, E_1), (t_2, E_2), \ldots\}$. Simultaneously, we measured the stress signal $\sigma(t)$ and, on the basis of that, we can define quantities also as a function of stress $\sigma(t)$.

Figure 1 shows the measurement setup and a single AE event. Time vs. stress curves from intact samples are shown in figure 2, which presents sample-to-sample variation in different experiments. The curves are shown both after scaling the sample strength (max. stress) and corresponding time to unity and in the usual way (inset). Both modes illustrate the sample-to-sample variation, and also in the proximity of the maximum stress. Figure 3 depicts time-stress-curves with a notch. As it is obvious, $\sigma(t)$ is of different shape and indicates stable crack growth.

3. Results

3.1. Temporal characteristics of the AE

We start our analysis from a time ordered set of time-event pairs from an experiment: $\{(t_1, E_1), (t_2, E_2), ..., (t_n, E_n)\}$. We divide the time interval (t_1, t_n) into windows of length Δt and compute the event energy rate $\dot{E}(t)$ and event count rate $\dot{n}(t)$ for acoustic emission in each Δt window defined according to equations 1 and 2.

$$\dot{E}(t) = \sum_i \frac{H(t - t_i)H(t_i - t + \Delta t)E_i}{\Delta t} \tag{1}$$

$$\dot{n}(t) = \sum_i \frac{H(t - t_i)H(t_i - t + \Delta t)}{\Delta t} \tag{2}$$

where $H(x)$ is the Heaviside step function.

After energy and event count rates have been obtained, these quantities are averaged over all experiments. For the averaging, we have to use a similar choice for the time axis (or stress) and there is no natural choice. The time $t = 0$ corresponds to triggering from the beginning of the tensile experiment, which is unphysical for any averaging. Before computing the average, we define origin of time and shift the signals $\dot{n}(t)$ and $\dot{E}(t)$ accordingly.

As a physical beginning of the experiment, the origin of time is defined as where we find the maximum slope of time-stress curve (see figure 2) and the intersection of the time axis and a straight line fitted to the point of maximum slope. This choice removes non-idealities at the beginning of the time-strain curve which often arise to experimental limitations, e.g. small slack in the sample when it is inserted to clamps. Figure 4 shows $E(t)$, the integral of event energy $\dot{E}(t)$, averaged so that the time is shifted to the beginning of experiments. The notched case shows stable crack growth. The unnotched energy integral depicts the onset of the acoustic emission when the plastic regime starts, but since time-to-failure scatters from sample to sample, the meaning of the average becomes subtle. The energy integral in the unnotched case is similar to the result presented in [6]. The differences between the result in [6] and figure 4 are due to the fact that latter does not include events after the stress has started to drop after maximum has reached, the larger scatter in failure times and the samples being more ductile. It is interesting to note that the data for the notched samples shows over two

orders of magnitude in integrated energy a power-law scaling $E_{cum} \propto t^{1.6}$. Assuming stable crack growth with a constant FPZ size, this feature could be interpreted as the crack length time dependence. Note that there is roughly one order of magnitude of difference between the samples without and with notches in total energy release magnitude.

Next we test for apparent criticality, which would imply the divergence of the event energy rate near a critical point that is, the finite lifetime of the sample (corresponding to maximum stress, or crack instability). Discussing this is meaningful only in the unnotched case, where one can see a rapid increase in the event energy near the maximum of the time-stress curve. Conventionally, the lifetime t_c is defined as the time at the maximum of stress $\sigma(t)$, that is $t_c|\max(\sigma(t))$. However we discover that the time at maximum stress t_c is different from the time at event the maximum of energy and event count rate $t_c'|\max(\dot{n}(t))$. Schematically these differences are shown in the Fig. 5. The sample to sample distribution of the quantity $(t_c' - t_c^*)$ is seen in figure 6 which shows that there is clear difference time at maximum event rate being larger. In other words, t_c' is found without exception after the maximum stress.

When we average quantities over samples by shifting the critical time to the origin before the averaging, as shown in figure 7, we find that event count rate $\dot{n}(t_c - t)$ appears to follow a power law according to Eq. (3), with the lifetime as $t_c|\max(\dot{n}(t))$:

$$\dot{n}(t_c - t) \sim (t_c - t)^{-\Delta} \tag{3}$$

where we find the value $\Delta = 1.4 \pm 0.1$. The error is defined using the min-max method.

Equation (3) does not apply for the event energy release rate $\dot{E}(t_c - t)$. A power law behaviour for the event count rate but not for the event energy implies a change in the average event energy during the experiment. This is shown in the figure 10: average event energy as a function of normalized stress σ/σ_{max} during the experiment. The result shows that there is rapid increase in the average event energy near σ_c. We can also look at event and energy rates as functions of normalized stress $(\sigma_c - \sigma)/\sigma_c$ as shown in figure 8. The cumulative event count shows over a range of rescaled stresses an apparent power-law dependence. The cumulative event energy behaves in a way similar to what was found by Garcimartin *et al* [13], but a power-law dependence is not clear, when we have the cumulative count as a reference.. The comparison is not straightforward due to different loading modes. The connection is further explored in the Discussion. As expected (on the basis of equation (3)) the event rate does not seem to scale here in any particular fashion.

3.2. Probability distributions of AE

Next we study statistical distributions of event energies E_i and inter-event times. Inter-event times in an experiment are defined as set of $\tau_i = t_{i+1} - t_i$. These exhibit almost without exception power-law statistics such that one defines probability distributions

$P(\tau)$ and $P(E)$ for the inter-event/waiting times and energies which are characterized by power-law exponents α and β, respectively according to equations 4 and 5.

$$P(E) \sim E^{-\beta} \tag{4}$$

$$P(\tau) \sim \tau^{-\alpha} \tag{5}$$

We find values $\beta = 1.4 \pm 0.1$ and $\alpha = 1.3 \pm 0.2$ for event energies and inter-event times respectively. However, interpretation of these statistical distributions is difficult since a typical tensile test (or fatigue or creep test) is not stationary. The internal state of the material changes along the whole test duration, and statistical quantities such as $P(E)$ or $P(\tau)$ integrate over the whole history of a sample. Thus we study how these statistical distributions change e.g. in relation to t_c or event count rate $\dot{n}$.

In figure 9 we show waiting time distributions from tensile experiments as a function of the event rate $\dot{n}$. The event rate $\dot{n}$ is computed in a window. Windows are divided into different classes on the basis of an event rate. The data sets in the figure represent waiting time distribution in the event rate class. The data set label indicates the averaged event rate in units of s^{-1} in the event rate class. Event rate classes are defined so that each class contains approximately 20 000 events. The difference between panels is the algorithm which identifies events: algorithm used in the lower figure allows overlapping of AE events while upper does not. The implication is that the algorithmic details are not important and differences we see in distributions is not due to the clustering of events at larger event rates. From waiting time distributions, it appears that there is a complicated change of the waiting time distribution $P(\tau)$ as a function of event rate though one must be careful as the window size is still (in the time-domain) relatively large compared to t_c. Perhaps, one can see signs of two different power-laws. It is interesting to note that the purest power-law behavior is obtained at small event rates (small strains) while for larger ones it changes to a more complicated distribution.

The energy distributions are shown in figure 11. Due to large variation in the average event size (see figure 10) near time at maximum stress, we studied changes in the probability density $P(E)$ close to t_c. The distribution in the Fig. 11 contains events up to the time $t_c - t'$. The time shift t' is shown in the label of the data set. The number of events is 6448 if we choose all events up to 10 seconds before t_c, and 162425 for all cumulated events up to 1 second after t_c. Despite the large increase in the average event energy, overall form of the probability density function does not change as much as $P(\tau)$ changes as a function of the event rate. Large event energies are cut off, when one considers the distribution which contains events up to the time which cuts off events after the event size has started to increase.

3.3. Theoretical models

In this chapter we compare experimental results to a random fuse network with a residual conductivity (RRFN). The model is analogous to the one proposed by Duxbury and Li [12]. It is a minimal quasi-static model for fracture, which includes stress enhancements

and residual bonding, leading to apparent plasticity and crack arrest. The model is an electrical analogy of an elastic lattice. The main motivation for using RRFN is that usual RFN simulations are much further away from the experiments.

In the model we connect a set of fuses to a square lattice with a size $L \times L$. Fuses are labeled as index j and associated with a constant conductivity $g_j = 1.0$ and with randomly distributed critical currents i_j^c. The distribution is uniform and characterized by its width: $i_j^c \in [1 - W, 1 + W]$. For the breaking process we apply a slowly increasing voltage across the lattice until the hottest fuse approaches its critical current i_j^c. The important ingredient over the usual RFN is that fuses break at two phases: at the first phase its conductivity drops from $g_j = 1.0$ to a residual conductivity $g_j = r$. The fuse remains non-broken in the network with a residual conductivity until its current threshold is exceeded again and then its conductivity drops to zero, which finally corresponds to breaking the fuse and generating an event. We apply this rule to the conductivity of the hottest fuse and start increasing voltage from zero again. The process of applying conductivity drops and re-evaluating the hottest fuse is repeated until the conductivity of the network goes to zero and burned fuses form a percolating path across the lattice.

When the residual conductance approaches unity, the model is identical to the perfectly brittle random fuse network. When the residual conductance is close to zero, stress enhancements create very tough fuses which are capable of arresting cracks and leading to plasticity. Width of the disorder parameter W leads to competing effect of the disorder and stress enhancements.

By finding VI-characteristic of the whole network, we obtain an entity which corresponds experimental stress-strain curves. We record a voltage-current pair (V_i', I_i') when a fuses conductivity drops to zero. We apply voltage-control for the ordered set $\{(V_i', I_i'), ...\}$ by requiring that when the voltage V_i' overcomes the highest value previously recorded we get one point for the VI-curve (V_k, I_k), where k identifies an "acoustic emission" event. In the Fig. 12 we show all voltage-current pairs V_i', V_i' from one numerical experiment and the envelope corresponds to the VI-curve $\{(V_k, I_k), ...\}$. In the Fig. 13 are voltage-controlled VI-curves from 99 simulations for the system size 124.

The event count rate is defined similarly as in experiments. We divide voltage-axis ΔV sized windows and compute number of events in a window according to Eq. 6. V_{max} is the voltage when the current is in its maximum. The "acoustic emission" event in this model is associated to second conductivity drop of the fuse, i.e. when the conductivity drops to zero. Creating an event from all conductivity drops was also calculated, but this did not lead to an acceleration of the event rate.

$$\dot{n}(V/V_{max}) = \frac{\sum_k H(V - V_k)H(V_k - V + \Delta V)}{\Delta V} \tag{6}$$

We performed set of simulations from system sizes 30×30 up to 124×124. The combination of disorder parameter $W \approx 0.8$ and residual conductivity $r \approx 0.2$ led to similar VI-characteristic as in experiments: activity started after the experiment

approached half of the critical voltage and we observed activity after the maximum voltage was approached (Fig. 13). This implies that even large cracks are arrested before a dominating crack is formed.

Fig. 14 shows the event count rate as a function of V/V_{max} averaged over 99 experiments. The event count rate starts to increase after 50% of the maximum voltage is approached. The event rate is in its maximum near V_{max}. There is a small tail in the event count rate after the maximum stress, which becomes steeper when the system size increases. The increase in the event count rate is neither a power law nor critical. In the Fig. 15 there is the histogram of the maximum event rate a a function of V/V_{max}. This depicts the difference between experiments and simulations: the maximum event rate occurs before or at the maximum current in simulations while in experiments it is observed after the maximum stress. However, there are still a few occurrences of the maximum event rate after the maximum current in simulations. We conclude that the time at the maximum event rate and the time at the maximum current are not identical. However, the relation is inverse to the experiment.

4. Discussion

We have compared fracture precursors using different "critical points" $t_c|\max(\sigma_c)$ and $t'_c|\max(\dot{n})$ in mode I loading and imposing a constant strain rate for copy paper samples.

A divergence is observed in samples without a notch, using time as a control parameter and looking at the event rate when approaching time at the maximum event rate. We have shown that the characteristic behaviour of the event rate $\dot{E}$ is different from the event rate $\dot{n}$. The behaviour of the event rate $\dot{n}(t_c - t) \sim t^{-\Delta}$ might be taken to imply criticality, when t_c is chosen to be the time at the maximum of the event rate. We note that the maximum of the event energy and event rate corresponds to a time which is observed after the maximum of the stress σ_c.

A plausible argument to explain the causal nature of the AE observations (without a notch) is as follows. At the maximum stress it follows that $\partial_\epsilon \sigma = E_\epsilon \epsilon + E$ becomes negative. Thus E_ϵ is negative, which could be taken to indicate that one of the microcracks dominates and has started to grow. The event rate increases with the crack growth velocity, till the crack instability takes place. The divergence of the event rate could be then arise from a divergence of the crack velocity. The relation of the rate divergence and the concomitant increase of the event energy release presents a complicated problem. The rate of energy release rate should (recall we assume here a single propagating, stable crack) to be proportional to the new fracture process zone (FPZ) area created (if the AE event energy is related to the new FPZ area multiplied by fracture toughness). However, we have shown that the diverging quantity seems to be the event rate and not the event energy, in such strain imposed loading.

Earlier experimental studies have shown indications of an event energy divergence when one imposes a constant pressure rate to a heterogenous material [14, 13, 15]. The critical exponent γ in $\dot{E} \sim \left(\frac{p-p_c}{p_c}\right)^{-\gamma}$ was found to be $\gamma = 1.4$ in [14], $\gamma = 1.27$ in [13]

and $\gamma = 1.0$ in [15]. In the case of an imposed constant strain rate there was not found to be any critical divergence of the energy release rate [16]. The analysis however was not done in the same spirit, and excluded the mechanism suggested above. Finally it was suggested that the real control parameter is time, since both imposing constant or cyclic stress seems to imply a critical divergence of the event energy [17]. Our results include a somewhat similar behavior for the event energies as the maximum stress is approached.

Statistical distributions of event energies $P(E)$ and inter-event times $P(\tau)$ have been measured earlier several times from paper. Power laws have been found with exponents $\beta = 1.4 \pm 0.1$ and $\alpha = 1.3 \pm 0.2$ for event energies and inter-event times, respectively. We may contrast the current result to earlier work by Salminen et al. where acoustic emission has been measured from paper in the machine direction [6]. The energy exponent β is here slightly larger, compared to $\beta = 1.25 \pm 0.10$, which might be attributed to the much more ductile nature of paper as a material when stressed in the cross-machine direction. The waiting time exponent α is almost identical when it is integrated over whole experiment.

In any case, in general most of the statistical signals that have been explored experimentally are still awaiting for theoretical explanations. For e.g. $P(E)$, brittle fracture models allow to derive power-law -like scaling forms but with exponents β that are in general far too large. To see if qualitative agreement could be found we compared the event rate from experimental data to the residual random fuse network. The event rate was found to increase when the voltage at maximum current was approached - contrary to perfectly brittle ordinary RFN. The result was not power-law divergence as in the experimental data. Note that introducing fracture toughness (residual fuses) to the model caused a change to the behaviour of the form of the event count rate: rapid increase of the event energy at V_{max} was not found in the perfectly brittle RFN model. Further studies of the RRFN would seem to be of interest. Note that Amitrano and Helmstetter [18] have proposed a numerical model in order to model time-dependent damage and deformation of rocks under creep. In the model the 2D finite element method is used and separate time-dependent and time-independent damage progression and time-to-failure laws are introduced. Time-independent damage progression on an element is introduced as a gradual drop of an elastic modulus if the stress threshold was exceeded: $E_i(n+1) = E_i(n)(1-D_0)$ where $E_i(n)$ is elastic modulus of an element after n damage events and D_0 is a constant damage parameter. Quasistatic stress redistribution may induce an avalanche of damage events during a single loading step. The damage progression law and quasistatic stress redistribution is similar to conductivity drop and re-evaluation of the voltage in RRFN. The difference is in the damage law of an element. The result of the model is a power-law acceleration of the strain rate $\dot{\epsilon}$ and the rate of damage events $\dot{n}$ near the failure time t_c. However, if we look at number of events as a function of strain $\frac{\dot{n}}{\dot{\epsilon}} \sim \frac{1}{(t_c - t)^{\gamma *}}$ the rate of damaged events decreases when t_c is approached. The result is qualitatively in agreement what is observed on the residual random fuse network when it is assumed that every conductivity drop creates an acoustic

emission event. The gradual failure does not explain the event rate acceleration near the failure in the experiments.

Eq. (3) is in essence identical to the Omori's law of aftershock rates. In the stationary paper peeling experiment one observes Omori's law with exponent close to $\Delta = 1.4$ and it is also comparable e.g. to tectonic seismicity. In that case the generic temporal properties are further discussed in Ref. [11]. Approaching a"main shock" in stationary experiment might be identical to approaching time at the maximum event rate in strain-driven non-stationary fracture experiment when we consider the behaviour of the event rate $\dot{n}$. Fundamental differences of non-stationary and stationary AE signals are the different forms of the inter-event time distribution and the increase in the average event energy before failure (or main shock). However, this acceleration of the event rate in the stationary experiment is significant when averaging over a large number of sequences and the similarity may be coincidental.

The limitation of the experimental setup is the limited choice of loading modes and lack of feedback control of the imposed strain or the stress. For example, driving material based on the acoustic emission event rate, as applied for the rock fracture in Ref. [19], we could obtain an experimental test to the criticality and diverging quantities of the paper fracture; it would be interesting to see if it is possible to alter the event rate divergence near t_c by controlling the strain based on AE feedback during an experiment.

Acknowledgements - The authors would like to thank for the support of the Center of Excellence -program of the Academy of Finland, and the financial support of the European Commissions NEST Pathfinder programme TRIGS under contract NEST-2005-PATH-COM-043386. Discussions and/or collaborations with Amandine Miksic and Lauri Salminen are also acknowledged.

[1] A. Petri, G. Paparo, A. Vespignani, A. Alippi and M. Constantini, *Experimental evidence for critical dynamics in microfracturing processes*, Phys. Rev. Lett. **73**, 3423 (1994).

[2] C. Maes, A. Van Moffaert, H. Frederix and H. Strauven, *Criticality in creep experiments on cellular glass*, Phys. Rev. B **57**, 4987 (1998).

[3] M.J. Alava and K. Niskanen, *The Physics of Paper*, Rep. Prog. Phys. **69**, 669 (2006).

[4] Y. Nakumara, C.L. Veach and B.O. McCauley, *Acoustic Emission*, STP-505, (1972); H. Corte and O. Kallmes, *Formation and Structure of Paper*, Mech. Eng. Publ. Ltd. London, 351 (1962).

[5] J. Sethna, K. Dahmen and C. Myers, *Crackling Noise*, Nature **410**, 242 (2001).

[6] L. I.Salminen, A.I. Tolvanen and M. J Alava, *Acoustic Emission from Paper Fracture*, Phys. Rev. Lett. **89**, 185503 (2002).

[7] M. J. Alava, P. K. V. V. Nukala and S. Zapperi, *Statistical models for fracture*, Adv. Phys. **55**, 349 (2006).

[8] J. Rosti, X. Illa, J. Koivisto and M.J. Alava, *Crackling noise and its dynamics in fracture of disordered media*, J. Phys. D: Appl. Phys. **42**, 214013 (2009).

[9] F. Finck, M. Yamanouchi, H-W. Reinhardt and C.U. Grosse, *Evaluation of mode I failure of concrete in a splitting test using acoustic emission technique*, Int. J. Frac. **124**, 139 (2003).

[10] L. G. Tham, H. Liu, C. A. Tang, P. K. K. Lee and Y. Tsui, *On Tension Failure of 2-D Rock Specimens and Associated Acoustic Emission*, Rock Mech. Rock Engng. **38**, 1 (2005).

[11] J. Rosti, J. Koivisto, P. Traversa, X. Illa, J-R. Grasso and M.J. Alava, *Line creep in paper peeling*, Int. J. Fract. **151**, 281 (2008).

[12] Y. Li and P. M. Duxbury, *Crack arrest by residual bonding in resistor and spring networks*, Phys. Rev. **B38**, 9257 (1988).

[13] A. Garcimartin, A. Guarino and S. Ciliberto, *Statistical Properties of Fracture Precursors*, Phys. Rev. Lett. **79**, 3202 (1997).
[14] A. Johansen and D. Sornette, *Critical ruptures*, Eur. Phys. J. **B18**, 163 (2000).
[15] H. Nechad, A. Helmsletter, R Guerjouma and D. Sornette, *Creep ruptures in heterogenous materials*, Phys. Rev. Lett. **94**, 045501 (2005).
[16] A. Guarino, A. Garcimartin and S. Ciliberto, *An experimental test of the critical behaviour of fracture precursors*, Eur. Phys. J. **B6**, 13 (1998).
[17] A. Guarino, S. Ciliberto, A. Garcimartin, M. Zei and R. Scorretti, *Failure time and critical behaviour of fracture precursors in heterogeneous materials*, Eur. Phys. J. **B26**, 141 (2002).
[18] D. Amitrano and A. Helmstetter, *Brittle creep, damage and time-to-failure in rocks*, J. Geophys. Res. **111**, B11201 (2006).
[19] J. Davidsen, S. Stanchits and G. Dresen, *Scaling and Universality in Rock Fracture*, Phys. Rev. Lett. **98**, 125502 (2007).

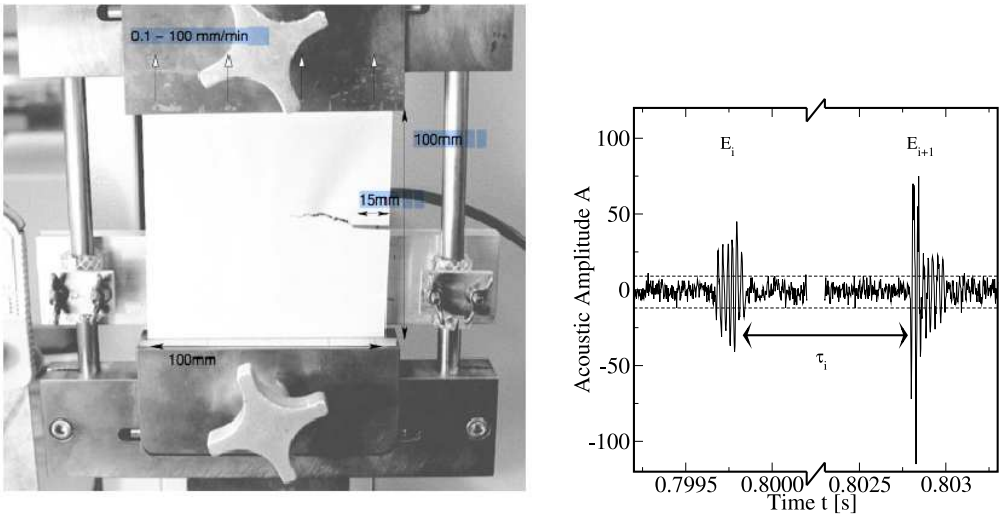


Figure 1. The measurement setup: sample attached to MTS tensile testing machine. In this Figure single piezocrystal sensor is attached to back of the sample (actual setup consisted two piezocrystals). The figure on the right shows single AE event signal [6].

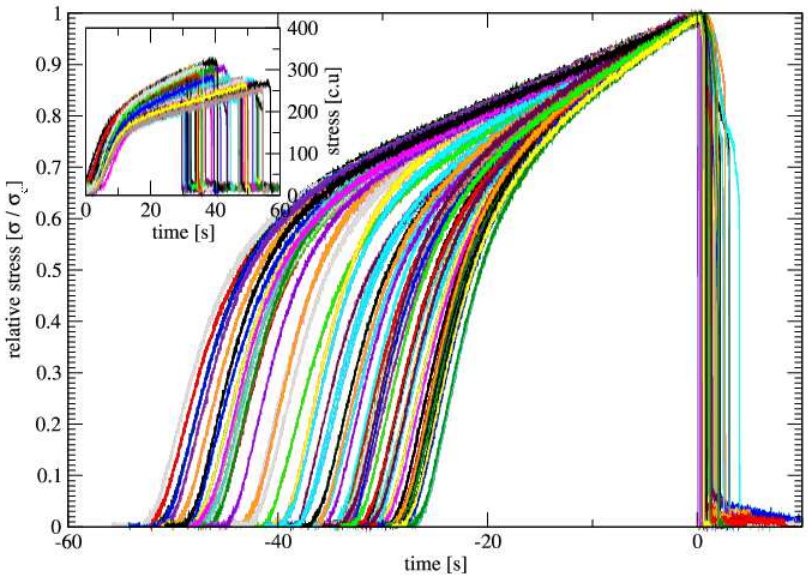


Figure 2. Time vs. stress curves from all samples without notch. The maximum stress is scaled to unity using σ/σ_c. This figure depicts typical stress response and its variations as a function of time. The inset contains same data without scaling of the

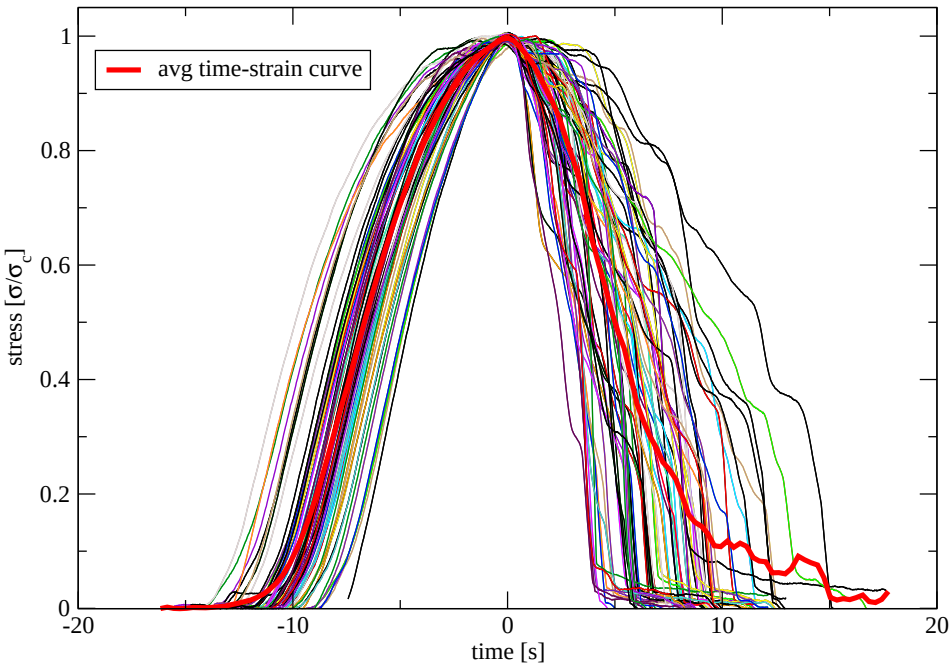


Figure 3. Time vs. stress curves from all samples with a notch. The maximum stress is scaled to unity using σ/σ_c. This figure depicts typical stress response of notched samples. Average over all time-stress curves is shown.

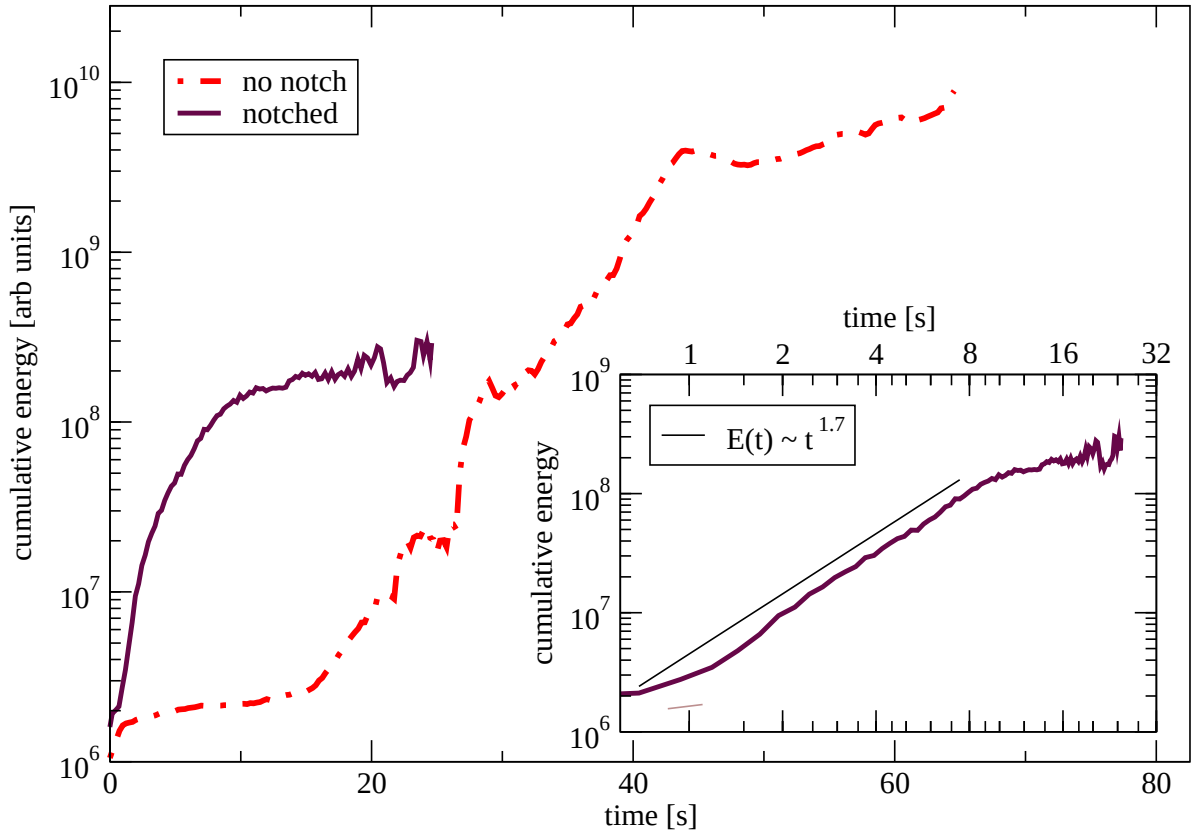


Figure 4. Averaged cumulative event energies as a function of time from the beginning of the experiment. The data is averaged over 100 and 70 samples. The notched case presents a power law increase of acoustic emission energy. The unnotched highlights the onset of acoustic emission, when the plasticity starts.

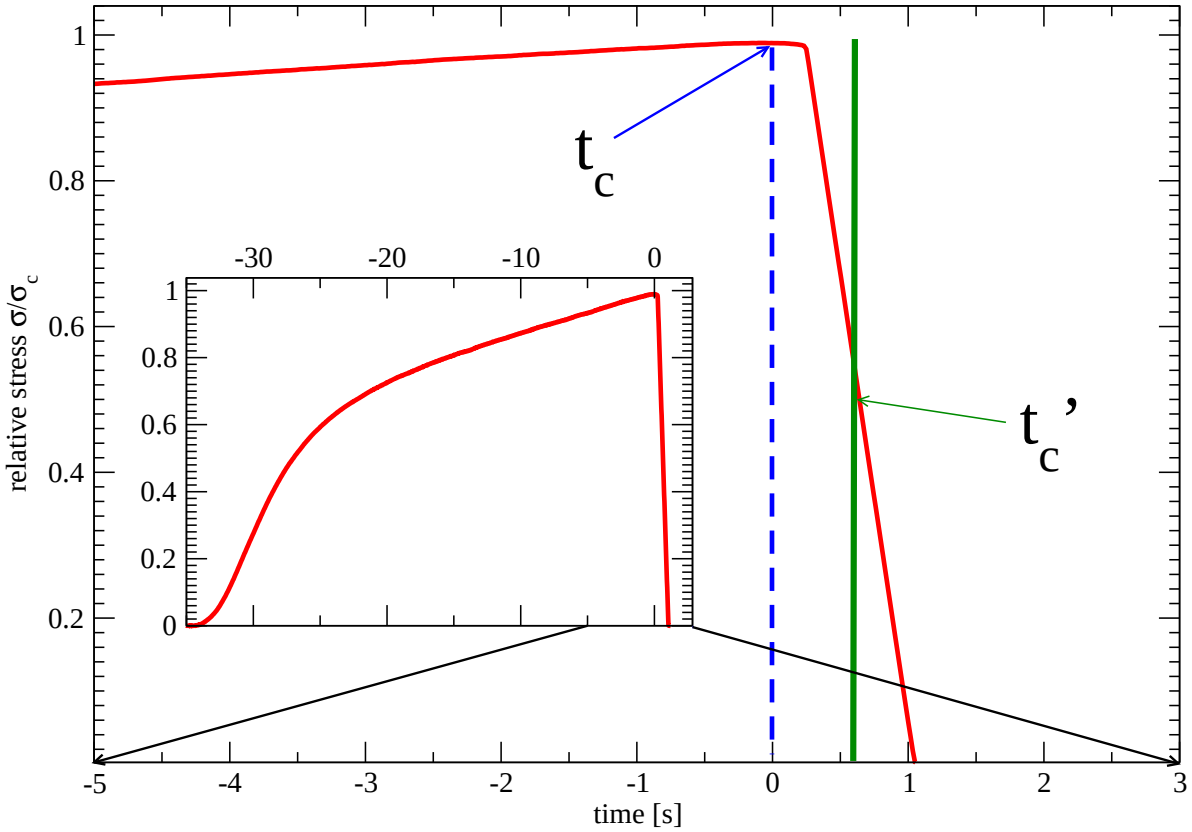


Figure 5. Schematic differences of $t_c|\max(\sigma(t))$ and $t'_c|\max(\dot{n}(t))$ in a single experimental time-stress curve. Inset shows time-stress-curve and main panel is magnified to the end of the experiment.

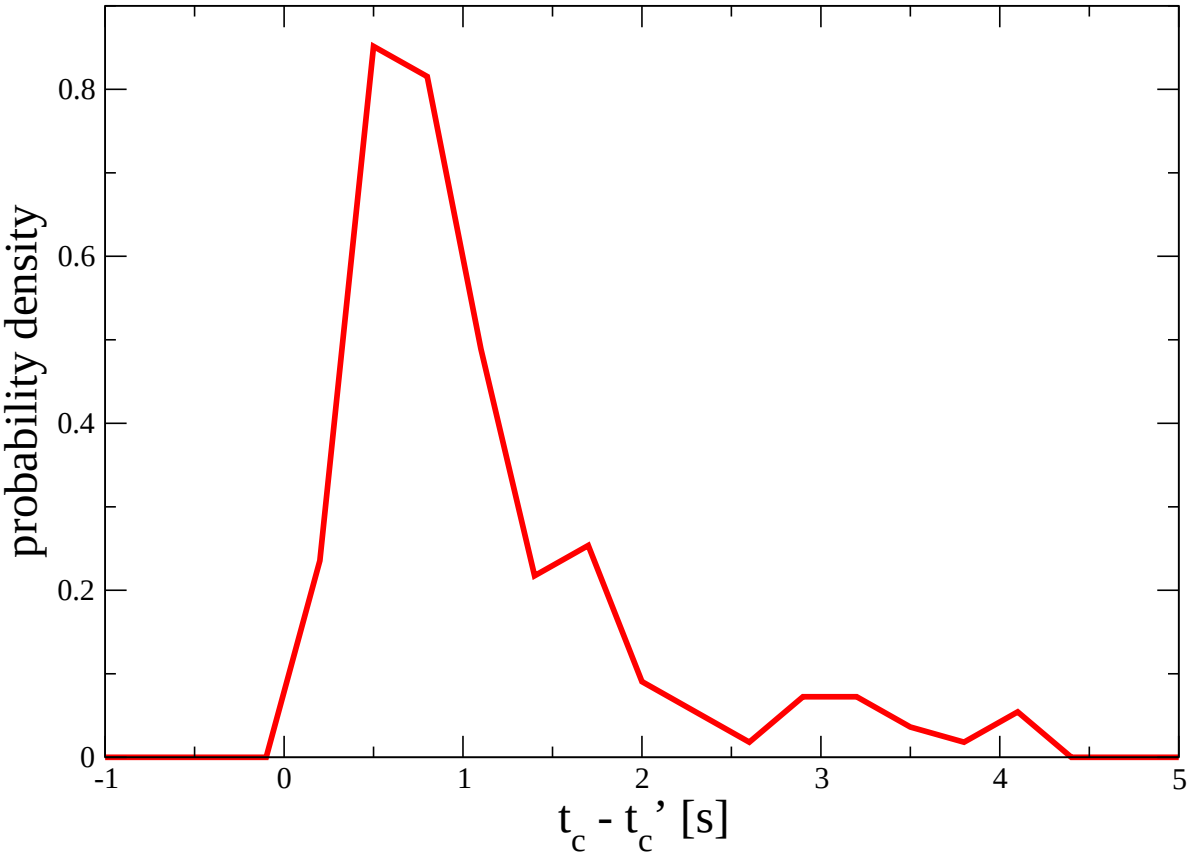


Figure 6. The distribution of $t_c'|\max(\dot{n}(t)) - t_c|\max(\sigma(t))$. The result indicates that time at the maximum of the event rate is larger than the time at the stress maximum.

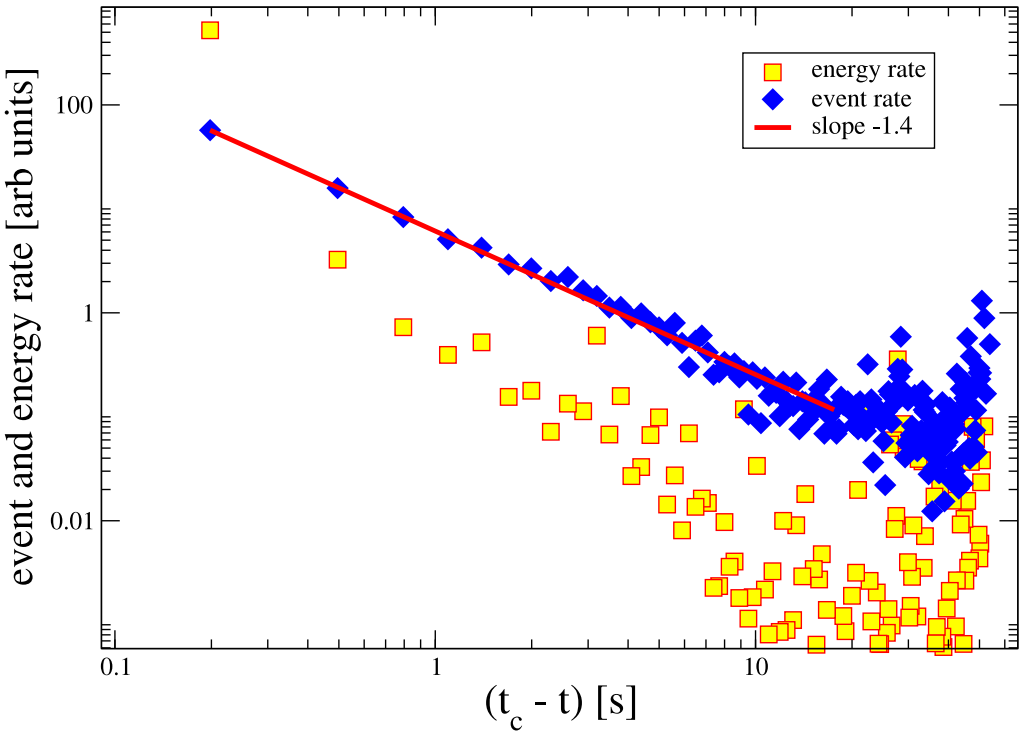


Figure 7. The event energy release rate $\dot{E}$ and the event rate $\dot{n}$ as a function of $t_c - t$. Energy release and event rates are computed in a window Δt=0.2s which is slided over AE time series. Critical time t_c is defined as a time where the energy relase rate $\dot{n}$ reaches its maximum value. Event energy and event rates are averaged over 100 experiments using AE from unnotched samples. The event rates decay as a power law, which is not true for event energies.

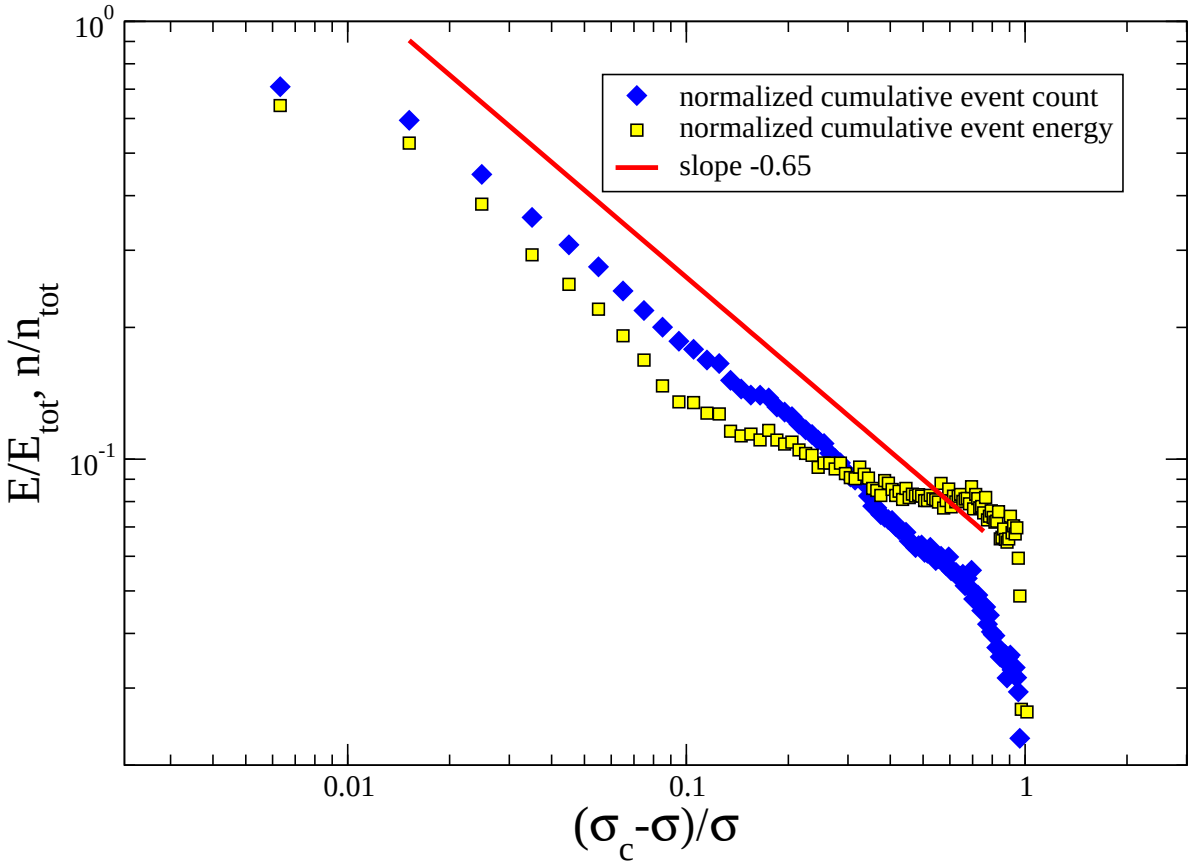


Figure 8. Cumulative energy E/E_{tot} and cumulative event count n/n_{tot} as a function of $\frac{\sigma_c-\sigma}{\sigma_c}$. Event energy and event counts are averaged over 100 experiments using AE from unnotched samples.

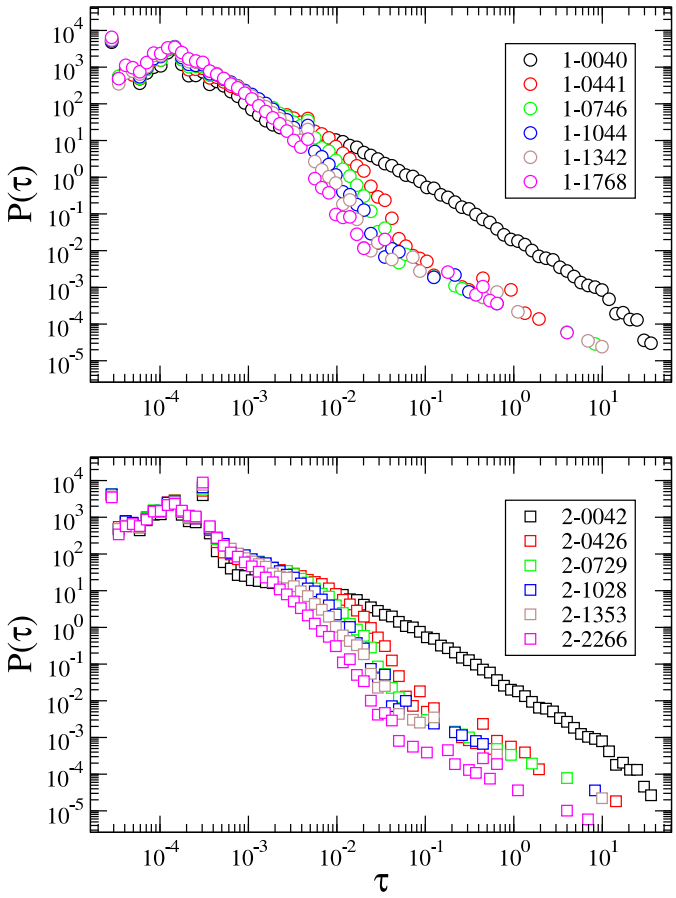


Figure 9. Waiting time distributions from tensile experiments. AE time series are divided to Δt=0.2 second time windows and waiting times τ_i and the event rate $\dot{n}$ is computed in a window. Windows are divided to different classes based on an event rate in the window and the data set in the figure indicates waiting time distribution in the event rate class. Label is the averaged event rate in the event rate class.

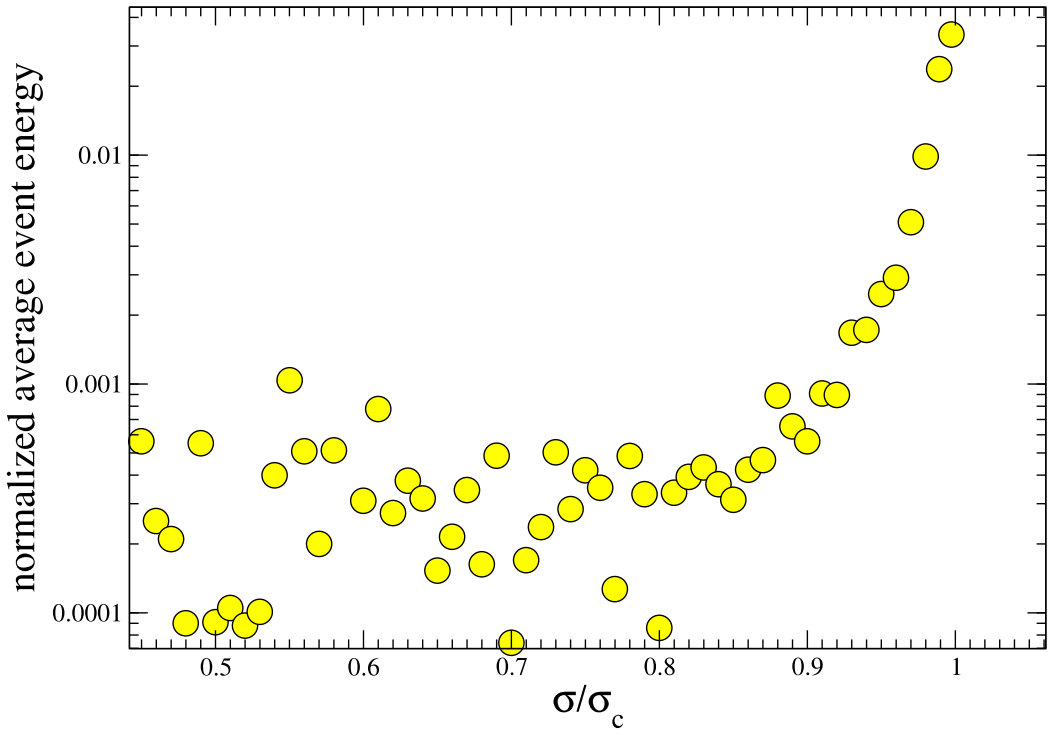


Figure 10. Average event energy, $\frac{\dot{E}}{\dot{n}}$, as a function of σ/σ_c. This result shows that the event energy is not constant during the experiment.

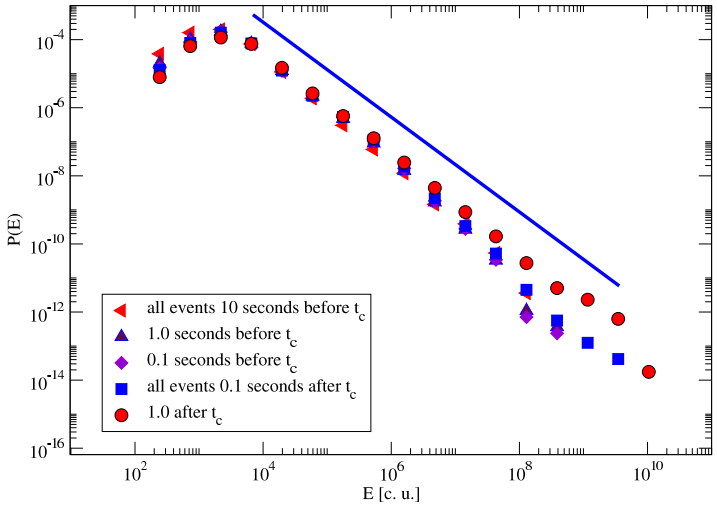


Figure 11. The figure depicts evolution in the probability density of event energies when the time at the maximum stress t_c is approached. The distribution contains events which are cumulated up to the time $t_c - t'$. The time shift t' is shown in the label.The distribution becomes broader when the maximum event rate is approached. The solid straight line is a power-law fit $P(E) \sim E^{-1.4}$.

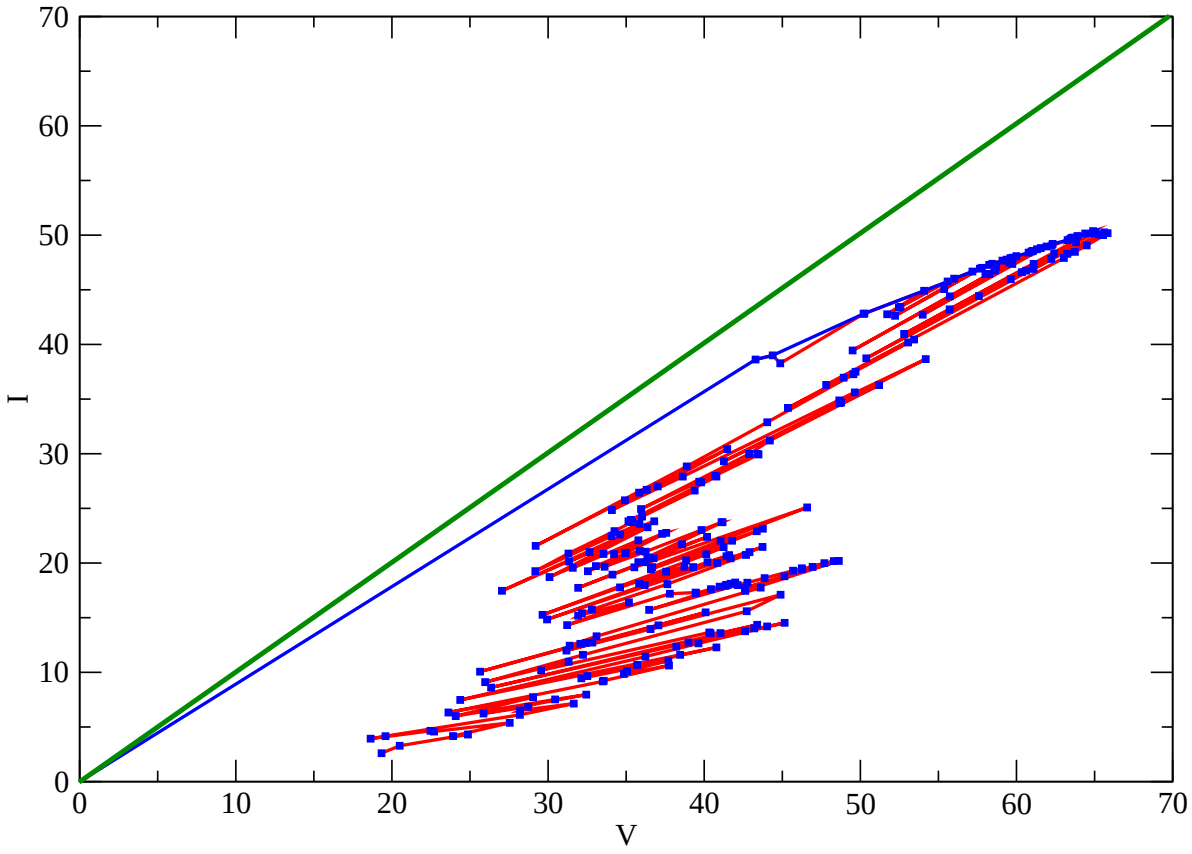


Figure 12. Voltage-current pairs from single RRFN simulation. System size is $L = 124$, disorder parameter is $W = 0.8$ and residual conductivity $r = 0.2$. Filled squares indicate VI-pairs when a fuse is burnt, that is its conductivity drops to zero. The straight line corresponds linearly elastic behaviour. The envelope curve corresponds stress-strain curve of the numerical experiment.

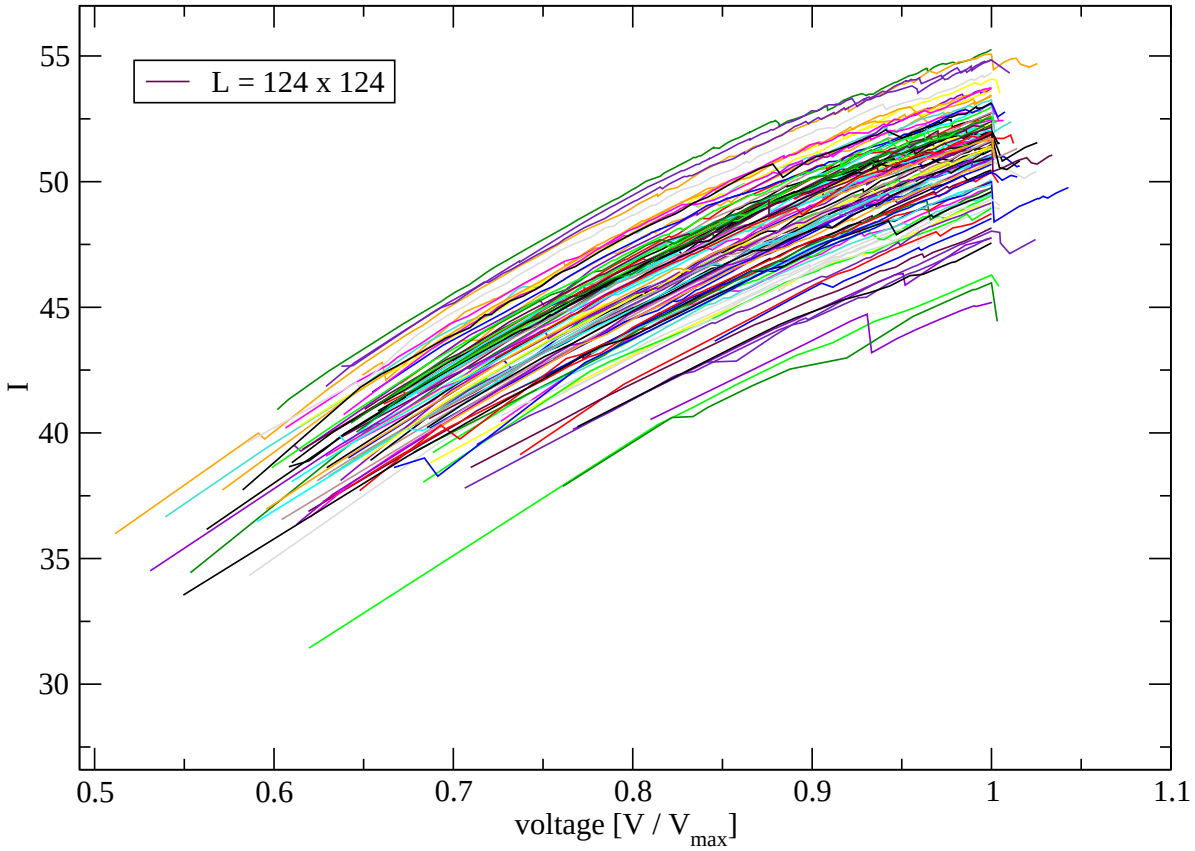


Figure 13. 99 voltage controlled VI-curves from RRFN simulations with system size $L = 124$. The disorder parameter is $W = 0.8$ and residual conductivity $r = 0.2$. The behaviour correspond qualitatively experimental stress-strain curves.

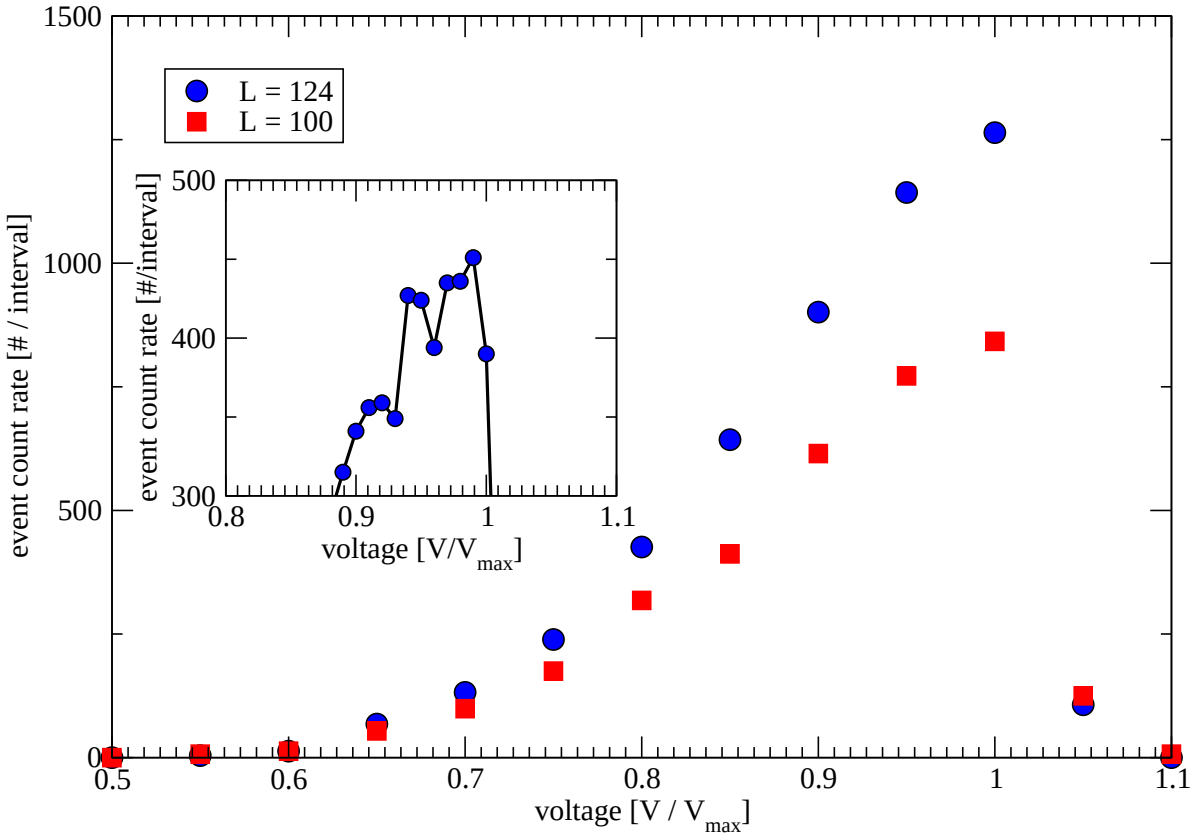


Figure 14. Event count rate near critical voltage from RRFN simulations. The data is averaged over 99 samples. Disorder parameter is $W = 0.8$ and residual conductivity $r = 0.2$. Increase in the event count rate is neither exponential nor a power-law. The tail of the event rate after the maximum current becomes steeper when the system size increases. The inset is a magnifigation of data with ten times smaller bin than in the main figure.

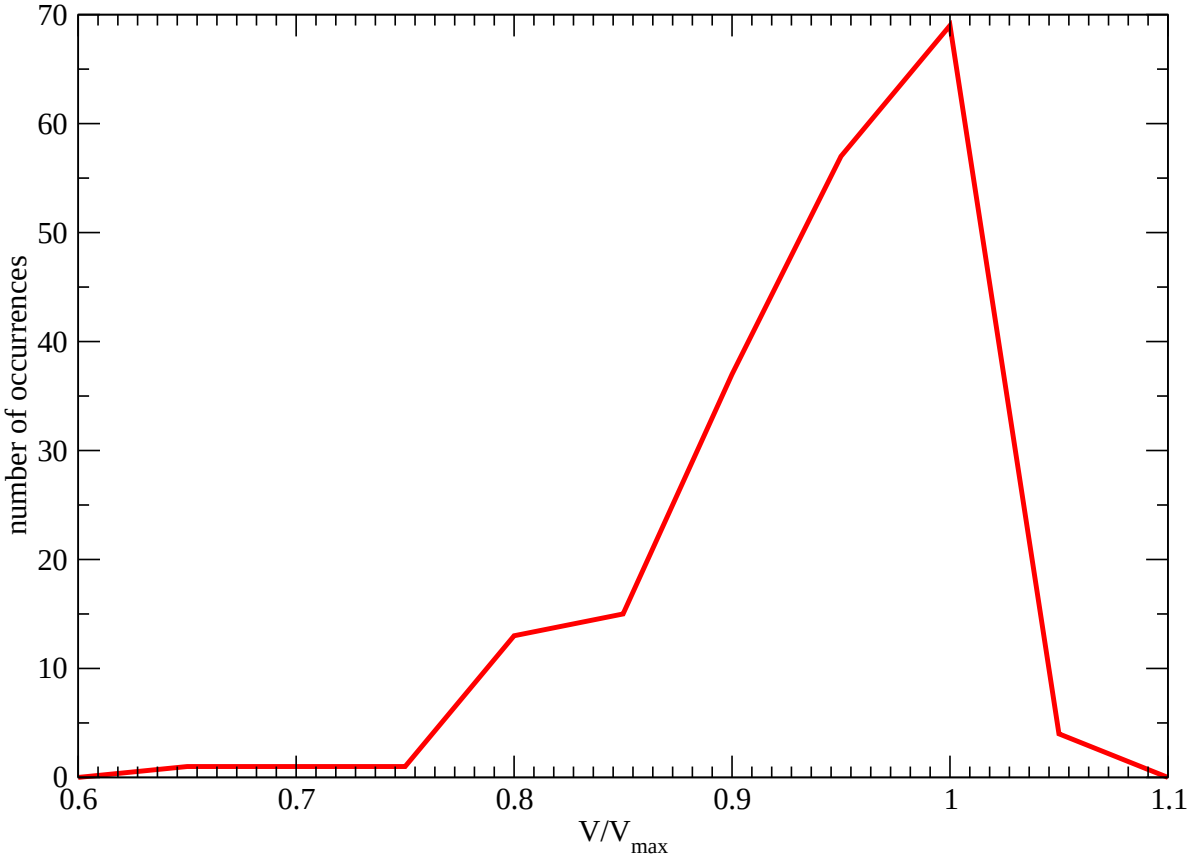


Figure 15. Histogram of maximum event rate occurrence as a function of V/V_{max}. The result shows sample to sample variation of the relative location of the event rate maximum. Histogram is from $L = 124$ and it contains 99 samples.